ChemComm

Recent advances in coiled-coil peptide materials and their biomedical applications

Journal:	*ChemComm*
Manuscript ID	CC-FEA-08-2022-004434.R1
Article Type:	Feature Article

ARTICLE

Recent advances in coiled-coil peptide materials and their biomedical applications

Received 00th January 20xx,
Accepted 00th January 20xx

DOI: 10.1039/x0xx00000x

Michael D. Jorgensen, Jean Chmielewski*

Extensive research has gone into deciphering the sequence requirements for peptides to fold into coiled-coils of varying oligomeric states. More recently, additional signals have been introduced within coild-coils to promote higher order assembly into biomaterials with a rich distribution of morphologies. Herein we describe these strategies for association of coiled-coil building blocks and biomedical applications. With many of the systems described herein having proven use in protein storage, cargo binding and delivery, three dimensional cell culturing and vaccine development, the future potential of coiled-coil materials to have significant biomedical impact is highly promising.

1. Introduction

Engineered biomaterials have been studied extensively for numerous applications, such as drug delivery and tissue regeneration.[1–3] Peptide-based materials specifically have drawn attention for their programmability and biocompatibility.[4–7] The use of natural and unnatural amino acid building blocks allows for facile modification of the peptide sequence and generation of various secondary and supersecondary folds. The coiled-coil motif, for instance, has drawn substantial interest due to its clear sequence-to-structure relationship and ease of tunability.[8,9]

The coiled-coil structure is widely observed in nature, and plays an essential role in many biological processes, including DNA recognition and gene regulation. The coiled-coil motif is composed of two or more alpha-helices that wrap around each other to form a left-handed supercoil (Figure 1). Each alpha-helix contains heptad repeats (*abcdefg*), with the usually hydrophobic *a* and *d* residues influencing the oligomeric state of the coiled-coil from dimers to heptamers.[10–12] The *e* and *g* residues are commonly ionic, with complementary charges between individual helices within the coiled-coil, while the remaining positions (*b*, *c*, and *f*) are solvent exposed and are typically filled with hydrophilic residues.

With these well-established structural parameters, general guidelines to design *de novo* coiled-coils have been developed.[8,9] Meanwhile, others have drawn inspiration from naturally occurring coiled-coils, such as those found in the transcription factors GCN4 and Jun-Fos.[10,13,14] A few recent reviews on the use of these coiled-coil building blocks for higher order assembly have emerged in the past five years. These have been focused on the use of orthogonal coiled-coil sequences within a single chain to create coiled-coil protein origami,[15] the development of multicomponent peptide assemblies with coiled-coils as one example of many other peptide secondary structures,[16] the use of coiled-coils to mediate the assemble of protein structures,[17] a comparison of collagen mimetic and coiled-coil peptides for metal-promoted assembly,[18] and applications of coiled-coil materials in drug delivery.[19] This review focuses on a broader investigation of the range of strategies that have been employed to create higher order assemblies from coiled-coil building blocks, the reversible nature of coiled-coil assemblies, and a selection of their biomedical applications that emphasizes the future potential of this field. Throughout this review a number of coiled-coils are discussed, and these sequences can be found in Table 1.

2. Higher Order Assembly of Coiled-Coil Building Blocks

2.1 Design Strategies for Assembly

Starting with various oligomeric versions of the coiled-coil motif, a number of strategies have been developed to facilitate higher order assembly of the starting building blocks. These assembly approaches include integrating additional interactions within the coiled-coil sequences, including ionic and metal-ligand interactions, and engineering covalent linkages and hetero-oligomeric coiled-coils. Significant effort has been expended to understand and control the morphologies of these coiled-coil-derived materials as described below.

Ionic Interactions. A highly successful method to facilitate higher order assembly of coiled-coil peptides is through ionic interactions. For example, the Woolfson lab has used *de novo* designed dimeric to heptameric coiled-coils as building blocks (Figure 2A).[20] The peptides included charged residues at the

[a] *Address here.*
[b] *Address here.*
[c] *Address here.*
† Footnotes relating to the title and/or authors should appear here.
Electronic Supplementary Information (ESI) available: [details of any supplementary information available should be included here]. See DOI: 10.1039/x0xx00000x

termini to allow assembly in a head-to-tail fashion (Figure 2A). Specifically, a lysine or glutamate residue was installed at the C-terminus to complement either a glutamate or free amino group at the N-terminus, respectively. This approach to linear assembly led to immediate fiber formation in phosphate buffered saline (PBS, pH 7.4) (100 μM peptide) with trimeric to heptameric coiled-coil modules. To improve the organization, these assemblies were subsequently thermally annealed to produce different morphologies depending on the oligomeric state of the building block. For instance, the tetrameric peptide (**CC-Tet2-F**) transitioned to thicker fibers (from 60-65 nm to 130-135 nm in width), whereas the pentameric coiled-coil transitioned from fibers to broad, sheet-like structures. This difference in the two morphologies upon annealing may stem from the lack of a complete denaturation for both peptides, suggesting incomplete transitions when annealed. Interestingly, the annealing process of the hexameric coiled-coil, **CC-Hex-T**, produced highly ordered fibers (~70 nm) that allowed for the elucidation of the packing through X-ray crystallography, revealing a square packed arrangement.[20] Additionally, the hydrophobic channel present within the hydrophobic cavity of each pentameric, hexameric, and heptameric coiled-coil (50 μM) was used to sequester the hydrophobic dye 1,6-diphenylhexatriene. The trimeric and tetrameric coiled-coils, however, did not trap the hydrophobic dye presumably because the hydrophobic cores did not contain a cavity.

While Woolfson and coworkers designed *de novo* coiled-coils as described above, others have used naturally occurring peptide sequences to create ionic-based assemblies. Conticello and coworkers reported a heptameric coiled-coil based on the GCN4 transcription factor (**7HSAP1**).[21] These researchers also used a head-to-tail strategy, but, they employed the free C- and N-termini for assembly, with two arginine residues installed at the *f* position to limit lateral association. The peptide (2 mM) formed fibers (479 ± 93 Da/Å, Figure 2B) in MES buffer (10 mM, pH 6.0) and could trap the dye PRODAN within the hydrophobic cavity of the heptameric coiled-coil. Because of the arginine residues, these fibers were much thinner (3 nm) when compared to those of Woolfson (85 nm). The Montclare lab has studied coiled-coil assemblies derived from the cartilage oligomeric matrix protein (**Q**).[22] This pentameric coiled-coil was designed to include a positively charged histidine-tag at the N-terminus, lysine and arginine residues at the C-terminus, and glutamate and aspartate residues in the middle of the peptide to allow for staggered assembly of the coiled-coil building blocks. This design led to fibril formation at 10 μM **Q** (20-560 nm in diameter) in phosphate buffer (50 mM, pH 4) with a brick-layer-like organization of the coiled-coils (Figure 2C). The peptide also assembled in the presence of the hydrophobic dye curcumin (5:1 molar ratio of curcumin to peptide). Assembling in the presence of this dye was found to promote packing of the coiled-coils and increase the fibril diameter significantly (16.0 ± 5.6 μm). While some evidence indicated curcumin binding to the hydrophobic coiled-coil interior, the change in morphology also suggests potential binding between protofibrils. This is in contrast to Woolfson's and Conticello's works where the hydrophobic dyes had no effect on morphology.

Assemblies based on non-covalent interactions can also be reversible using pH. For instance, Conticello and coworkers installed histidine residues at the interior *d* position of the GCN4 trimeric coiled-coil (**TZ1H**). so that only deprotonated histidine would lead to coiled-coil formation (pH > 5.8).[23] Upon incubation in phosphate buffer (10 mM, pH 8.2), **TZ1H** (1 mg/mL) assembled into bundles of fibers (40–100 nm) over a period of 3 hrs (Figure 3A). Charged histidine residues, on the other hand, disrupted the coiled-coil structure by destabilizing the hydrophobic pocket, and the absence of this supercoil prevented the higher order assembly via ionic interactions from occurring. The fiber assembly and disassembly, therefore, was controlled through the addition of base or acid, respectively. Alternatively, Dexter and coworkers designed a highly charged *de novo* peptide with histidine, lysine, and glutamate residues at solvent exposed positions of the coiled-coil backbone (**AFD19**).[24] The peptide (1.75 mM), under conditions where the net charge was close to zero (pH 5.9), first formed fibrils due to misalignment of the helices producing overhangs, followed by hydrogel formation on a time scale of seconds to hours depending on the peptide concentration (Figure 3B). Highly charged versions of **AFD19** led to no assembly and a low viscosity solution. The researchers also demonstrated rapid hydrogel dissolution by adjusting the pH. The Chmielewski lab has also developed a coiled-coil assembly that is responsive to pH.[25] They introduced bipyridine moieties at the solvent exposed *f* position of a trimeric coiled-coil derived from GCN4. One to three bipyridines were installed on the coiled-coil peptide by substituting solvent exposed residues with lysine (D6K, S13K, and N20K) and subsequent bipyridine modification (**TriByp1**, **TriByp2**, and **TriByp3**). Incubation of the peptides (250 μM) in MOPS buffer (10 mM, pH 7.0) promoted radial association of the building blocks via aromatic interactions across the coiled-coils, leading to nano- to micron-scaled rectangular assemblies (Figure 3C). An increase in the number of bipyridine units led to a decrease in the aspect ratio of the assemblies (16:1 to 0.9:1). When subjected to acidic conditions (pH 3.0), the protonated bipyridine groups caused disruption of the coiled-coil interfaces, rapidly leading to dissolution of the assembly. The material could then reassemble upon addition of base, and this overall process went through numerous cycles without a change in the morphology of the assembly. Despite using different strategies, each lab created a pH-switchable material capable of assembly and disassembly on command.

Changes in pH may also lead to changes in morphology of the assembly. For instance, Montclare and coworkers investigated the hydrogelation properties of peptide **Q** (*vide supra*) as a function of pH.[26] At neutral and basic conditions (pH 7.4 and 10) a fiber-based hydrogel formed with **Q** (2 mM) in 96 and 24 hrs, respectively. Acidic conditions (pH 6.0), on the other

hand, led to polydispersed nanoparticles with no gelation after a two-week period (Figure 4A). This shift in morphology from fibers to nanospheres was due to an increase in electron repulsion of the highly charged coiled-coil. Pochan and coworkers have also found changes in morphology of the assembly of a designed coiled-coil peptide depending on the pH.[27,28] Acidic conditions (10 mM sodium acetate buffer, pH 4.5) led to nanotubes (21.3 ± 2.8 nm in length) with 1 mM peptide, while neutral (10 mM phosphate buffer, pH 7) and basic (10 mM borate buffer, pH 10) conditions led to stacked platelets (50-500 nm in length) and needles (100-250 nm in length), respectively (Figure 4B).[27] These notable differences arise from packing the coiled-coils so as to minimize electrostatic repulsion. In an acidic environment, the coiled-coils are tilted in the assembly to minimize electron repulsion of the positively charged free N-terminus. Under neutral conditions, the two-dimensional plates form through lysine-aspartate salt bridges whereas basic conditions weaken these salt bridges and lead to a primarily unidirectional assembly.

Overall, the examples provided above demonstrate that ionic-based assemblies are a simple yet powerful strategy to create a diverse range of structures. Loading of additional small molecule cargoes within the structures demonstrates potential for drug loading, and the developed feature of reversibility embedded within some of these materials may be harnessed for drug delivery as well.

Metal-ligand Interactions. The introduction of metal-binding ligands onto the coiled-coil scaffold has been shown to be a powerful technique to facilitate higher order assemblies. Early studies from Ogawa and coworkers installed a pyridine ligand at a centrally located, solvent exposed *f* position of a dimeric coiled-coil containing an IAALEQK heptad repeat (**AQ-Pal14**).[29,30] Complexation of the dimeric **AQ-Pal14** with platinum at 60 °C for a week was found to induce assembly into both nanometer-scaled globular structures and a smaller population of nanofibrils. In a subsequent study by Ogawa, the pyridyl alanine ligands were substituted with histidine (**H21**), and this dimeric coiled coil was treated with cobalt (III) protoporphyrin IX at 60 °C overnight.[31] Evaporating this solution for scanning electron microscopy (SEM) analysis showed that the mixture formed much larger fibrils than the previous study, presumably due to bis-axial ligation between the imidazole ligands of the dimeric coiled coil and a cobalt complex.[31]

Chmielewski and coworkers have successfully used metal-ligand interactions for assembly using a trimeric coiled coil building block based on the GCN4 sequence.[32–34] This design is different from the above work of the Ogawa in that the ligands for metal ions are at the termini of the peptide to promote head-to-tail assembly, rather than at a central heptad of the coiled-coil, and a trimeric module was used.[32] The peptide (**p2L**) contained nitrilotriacetic acid (NTA) and di-histidine ligands at the N- and C-termini, respectively. Addition of Zn(II), Cu(II) and Co(II) (0.4 eq) to **p2L** (1 mM) rapidly (30 min) provided well-ordered hexagonal crystals at room temperature, whereas 0.1 eq of zinc produced hexagonal disks. The crystal structure of the zinc-promoted crystals was solved and a hexagonal open-packed assembly was observed with the ligands directed towards the P3 face of the crystals (Figure 5A). Alternatively, nanospheres were observed with metal-mediated assembly using Ni(II), a morphology that was observed to some extent at much shorter time periods (5 min) with Zn(II), but which then evolved into crystals.[32] These researchers took advantage of the unsatisfied ligands within and on the P3 face of the growing and preformed crystals, respectively, to introduce His-tagged fluorophores with the crystals in a metal-dependent fashion.

Horne and coworkers have also studied metal-mediated coiled-coil assembly, but in their work, they used *de novo* designed sequences and terpyridine ligands. They investigated three different oligomerization states of the coiled-coil (dimer, trimer and tetramer), each with a different positioning of the ligand(s). For instance, the dimeric coiled coil (peptide **1**) contained terpyridines in the *f* position of the first heptad, and the *e* position of the last, whereas the trimeric peptide (**2**) had these ligands at the *a* and *c* positions of the first and last heptads. A tetrameric variant (peptide **3**) contained a single ligand at an internal *f* position. Although a number of divalent transition metals were investigated, only Cu(II) (3- 10 mM) was found to promote crystallization of the peptides (~2-4 mM, pH 6-6.5) using the hanging drop vapor diffusion method (time not indicated).[35,36] Crystal structures revealed that the Cu^{2+} ions bind to these ligands in addition to nearby glutamate residues (Figure 5b) yielding a complex packing arrangement for the peptides **1** and **2**, and a 2D net embedded in the lattice for **3** (Figure 5C). In an interesting comparison, **TriByp1/2/3** described above (250 μM, pH 7), which contained bipyridine ligands in central heptad repeats based on the trimeric coiled-coil of GCN4, did not require metal ions for assembly. The bipyridine ligands alone mediated aromatic interactions leading to a hexagonal, close-packed assembly of trimeric coiled coils after 48 hrs.[24]

Ogawa and coworkers introduced a single CXXC metal binding motif within oligomeric coiled-coils, with the Cys residues in the interior *a* and *d* positions of the coil.[37,38] Their goal was to form metal complexes inside an individual coiled-coil, however, and not promote higher order assembly of the building block. As described above, Conticello and coworkers, introduced His and Cys ligands also within the hydrophobic core of the coiled coil.[39,40] In their case, however, three His residues (**TZ1H**) or two Cys residues (**TZ1C2**) were introduced per helix. This allowed individual helices to form staggered coiled coils in a metal-dependent fashion. Higher order assembly into long aspect ratio fibers and fibrils were observed in the presence of Ag(II) (1 eq) with **TZ1H** (70 μM) or Cd(II) (2 eq) with **TZ1C2** (500 μM) (Figure 6A).

A strategy to use metal-ligand interactions to make highly crosslinked structures with coiled-coils for tissue engineering has also been investigated by Chmielewski and Jorgensen. In this case the central bipyridine moiety of **TriByp1** was combined with the NTA and His_2 ligands of **p2L** to create the peptide **TriCross**.[33] The use of ligands for metals at both the middle and ends of the coiled-coil indeed created a more complex metal-promoted assembly, with Zn(II), Ni(II), Cu(II), Co(II) (1 eq, 1 mM TriCross) producing a crosslinked three-dimensional (3D) mesh within minutes (Figure 6B). The matrix formed from **TriCross** contained micron sized cavities that were suitable for cell encapsulation (*vida infra*). An advantage of metal-mediated assembly is that the association can be abolished with

metal-chelating agents. For example, the formation of both the **p2L** (hexagonal crystals, Figure 5A) and **TriCross** (3D matrix, Figure 6B)) assemblies was found to be reversible through the addition of low levels of ethylenediaminetetraacetic acid (EDTA).[32,33]

Overall, integrating metal-ligand interactions within coiled-coil peptides is an important advancement in the field, especially as it pertains to the crystalline arrays and 3D matrices generated above. The use of metal ion-promoted assembly is a powerful means to rapidly generate crystals on demand and incorporate cargo in a metal-dependent manner. Additionally, the judicious placement of multiple ligands on the coiled-coil building block allowed for metal-promoted formation of a 3D scaffold that encapsulated cells simultaneously. A notable feature of this strategy for assembly is the inherent reversibility that is available for the dissolution upon treatment with chelators – a feature with interesting potential in tissue engineering.

Covalent Linkages and Heterocoiled-Coils. An alternate way to generate biomaterials from coiled-coil peptides is to link the building blocks together via covalent bonds. This has been accomplished in one set of examples by using different click chemistries. For instance, Woolfson and coworkers used native chemical ligation between hexameric coiled-coils. **CC-Hex-T**, described above, was optimized to minimize lateral association and maximize linear assembly (**CC-Hex-T + co**).[41] Native chemical ligation was used to link the building blocks using either two cysteine amino acids or two thioester moieties at each termini of a single coiled-coil. Rather than the previously described ionic driven assembly, the fibers that were generated (30-40 nm after 30 min and 100 nm after 1 week) were due to the covalent bond formed through the ligation chemistry to link the coiled-coils.

Similarly, Pochan and coworkers have used bond formation between coiled-coils using thiol and maleimide moieties. They used two tetrameric coiled-coils, one bearing terminal maleimides (**Peptide 1**) and the other flanked with cysteine residues (**Peptide 2**).[42,43] This design produced nanorods (>30 microns) with an alternating **Peptide 1** and **Peptide 2** pattern. Additionally, the Kirshenbaum lab has used the Huisgen cycloaddition for covalently linking coiled coils. In this case, the resulting triazole linkage was used to connect a dimeric coiled coil, based on the **SYNZIP** peptide, in a central position with 1-2 different dimeric coiled coil sequences (**4A** and **4B**).[44] Depending on the location of **4A** and **4B**, a barbell or quadrilateral assembly was observed. These strategies described above provide a facile route to design of coiled-coil materials based on chemical reactions.

Yet another covalent technique to induce higher order assembly is to install flexible peptide and polymeric linkers between helices of the coiled-coils. Jerala and coworkers, for example, elegantly designed a tetrahedron assembly using a mixture of homomeric and heteromeric coiled-coils with flexible peptide linkers (**TET12**).[45,46] The tetrahedron material was composed of a single polypeptide chain containing twelve coiled-coil domains each flanked with a flexible tetrapeptide spacer (SGPG) to prevent extended helix formation with a neighboring coiled-coil (Figure 7A). To confirm the topological fold of the peptide, the N- and C-termini of the polypeptide were grafted with split yellow fluorescent protein fragments that provided a strong fluorescent signal.

Tirrell and coworkers have used a triblock design to create an assembly from the protein **EPE**, with **E** representing an elastin-like sequence flanked with cysteines and **P** representing the coiled-coil sequence from cartilage oligomeric matrix protein.[47,48] The **EPE** protein was conjugated to a 4-arm PEG linker to initiate the crosslinked network. To control the strength and rigidity of the hydrogel, the strength of the coiled-coil was altered, either through sequence modification or the addition of denaturants. In a somewhat analogous study from Tirrell and coworkers, triblock peptides were investigated in which two coiled-coil forming peptides were connected with a peptide linker. In this example, a central random coil peptide was connected to a pentameric coiled-coil peptide from the cartilage oligomeric matrix **P** and a tetrameric coiled-coil peptide **A** (**PC10A**). This design generated a crosslinked network that was notably stronger (100-fold increase) when compared to the homodimeric counterparts (**AC10A** and **PC10P**).[49] Similarly, De Vries and coworkers used a self-assembling triblock linked to heterocoiled-coil peptides ($\mathbf{C_2\text{-}S^H_{48}\text{-}C_2\text{-}D^A}$ and $\mathbf{C_2\text{-}S^H_{48}\text{-}C_2\text{-}D^B}$).[50] Without the heterocoiled-coil building blocks, simple fibrils were observed at pH ≥ 6 from $\mathbf{C_2\text{-}S^H_{48}\text{-}C_2}$ alone. The installation of the coiled-coils, however, led to a heavily crosslinked morphology of the fibrils (Figure 7B). The degree of crosslinking was controllable by varying the density of coiled-coil labeled blocks.

Polymeric linkers have also been used to create more extensive structures with coiled-coils. Early work by Ghosh and coworkers used complementary alpha-helices that were conjugated to PAMAM dendrimers through cysteine-maleimide chemistry ($\mathbf{D\text{-}EZ_4}$ and $\mathbf{D\text{-}KZ_4}$).[51] Upon mixing the two peptide conjugates in phosphate buffer, the alpha-helices formed coiled-coils and created fibers (> 10 μm in length) after 8 hrs. More recently, Aili and Blank connected alpha helices to four-armed PEG linkers in a design to control the crosslinking properties.[52–54] Aili used dimeric coiled-coils with either isoleucine or valine at the *a* position ($\mathbf{pEV_4}$, $\mathbf{pEI_4}$, $\mathbf{PKV_4}$, and $\mathbf{PKI_4}$) to control the strength of the network by taking advantage of the coiled-coil binding affinities (Figure 7C).[52] The peptides were linked to the PEG polymer via Cys/maleimide chemistry, and hydrogels were formed with the peptide conjugates (250 μM) in phosphate buffer (pH 7) within hours. Hydrogels that were composed of only isoleucine coiled-coils (**PEI4**/**PKI4**) resulted in a stronger gel when compared hydrogels with both valine and isoleucine alpha-helices (**PEI4**/**PKV4**) (G' of 1000 Pa vs 200 Pa). Blank, on the other hand, controlled the strength of the crosslinked network through both covalent coiled-coil formation with a star-PEG polymer and metal-ligand interactions. Specifically, histidine ligands were installed at the solvent exposed *f* position of dimeric coiled-coil forming peptides ($\mathbf{A_{4H3}}$ and $\mathbf{B_{4H3}}$) to create a second layer of crosslinking.[53,54] The hydrogel formed without added metal ions (0.5 mM peptide conjugate, pH 8.1) exhibited a large linear viscoelastic range, whereas addition of zinc ions (1 eq) increased the degree of crosslinking and transitioned from viscoelastic to elastic-like gels. Similar to metal-mediated assemblies, the addition of

metal chelators like EDTA (4 eq) returned the hydrogel to its original state. While Aili explored the binding affinities of covalently linked coiled-coils to control the strength of the hydrogel, Blank used a covalent strategy in conjunction with a metal-mediated strategy to tune hydrogel properties.

The covalent strategies outlined above are a powerful means to swiftly link together coiled-coil peptides via various "click" reactions or with peptidic/polymeric linkers. These approaches lead to assemblies with morphologies that are often distinct from those obtained with the coiled-coil building block alone. The peptide origami approaches are an especially compelling example of the power of using heterocoiled-coils to tune stability and precisely control the resulting assemblies. The chemical approach allows for multiple modifications away from natural amino acids, whereas the ability to express the proteins, as in the case with the origami sequences, may provide a cost-effective way to generate the desired proteins.

2.2 Applications

Cargo Storage and Delivery. Perhaps the most studied application to biomaterials is cargo storage and delivery. While lyophilized powders remain the gold standard for protein storage, the lyophilization process can be harsh for the proteins and lead to degradation.[55,56] Meanwhile drug delivery remains a challenge and continues to be optimized to improve solubility of hydrophobic drugs, increase bioavailability, and minimize off target effects.[57–59]

Incorporating proteins within coiled-coil assemblies is one possible strategy to stabilize proteins. To this end, Chmielewski and co-workers used their **p2L** coiled-coil crystals described above to include proteins within the crystal. During the metal-mediated assembly, His-tagged protein guests were incorporated in an ordered fashion via metal-ligand interactions inside the crystal host in an hourglass pattern.[32] By incorporating His-tagged EGFP and derivatives inside the crystalline matrix, significant stabilization of the folded protein was achieved, even at 100 °C. These data demonstrate the potential of this assembly for room temperature storage of thermally sensitive proteins (Figure 8A).[34] In an alternate strategy, Clark and coworkers stabilized citrate synthase (CS) by incorporating the enzyme covalently in coiled-coil filaments.[60] These filaments were composed of the coiled-coil peptide building blocks **EE** and **KK** derived from the γPFD protein. While CS aggregates in solution at 43 °C, embedding CS in the filaments through covalent linkages stabilized the enzyme. These two coiled-coil peptide materials, while using different mechanisms of assembly, provide great promise for protein stabilization and may provide a scaffold for enzymes.

Cargo delivery using nanoparticles derived from coiled-coil assemblies has seen notable recent advances. The Xu lab has developed a micelle composed of a coiled-coil peptide with a poly(ethylene glycol) side-conjugate and a terminal hydrophobic tail modification (**1coi-dC18-PEG2K**, Figure 8B). In collaboration with the Ferrara and Bankiewicz labs, they investigated the numerous properties of the micelle nanoparticles for anticancer agent delivery.[61–68] For example, doxorubicin-loaded micelles were used to treat prostate and breast cancers in mice.[63] Later generations of these nanoparticles included trimeric and tetrameric coiled-coil species to control the location and cluster size of the drug on the micelle,[67] and cysteine modifications for redox reactive micelles.[68] Similarly, Kobatake and coworkers also reported drug delivery nanoparticles using a coiled-coil motif conjugated to an elastin-like peptide (ELP).[69] In this design, a heterocoiled-coil was used with helix A conjugated to single-chain vascular endothelial growth factor (VEGF) while helix B was conjugated to the ELP. Nanoparticle formation in the presence of paclitaxel created an anticancer delivery vehicle, whereby the external VEGF decoration directed the particles to the VEGF-receptor of cancer cells with paclitaxel ultimately causing cell death.

Different types of nanospheres have also been investigated for cargo delivery. Woolfson and coworkers have designed self-assembling cage-like particles (**SAGEs**) through a combination of heterocoiled-coil design and disulfide linkages (Figure 8C).[70–72] A homotrimeric coiled-coil (**CC-Tri3**) was linked to either alpha-helix **A** or **B** with a disulfide bridge, and subsequent mixing of the two sets led to **AB** heterocoiled-coil formation. Whereas the nanoparticles developed by Xu and Kobatake had hydrophobic cores, this **SAGE** has a hollow interior. **SAGEs** were modified at their termini with proteins (green fluorescent protein or luciferase) to decorate the interior or exterior of the cages without compromising the integrity of the material.[71] The cages were also modified to optimize cell uptake by introducing charged residues at the surface.[72] Stevens and coworkers, on the other hand, created nanoparticles using a layer-by-layer assembly on a colloidal surface.[73] The layers were generated with heterocoiled-coil components (**JR2EC** and **JR2KC**) linked to a polymer via cysteine-maleimide chemistry. Using this strategy, up to four layers could be assembled, with each layer containing trapped dextran. In this way, controlled release of cargo was accomplished through enzymatic degradation of each layer.

Coiled-coil assemblies using different morphologies have also been investigated as potential cargo delivery vehicles. Chmielewski and coworkers, for instance, generated nanotubes based on a trimeric GCN4 leucine zipper (**TriNL**) that selectively encapsulated fluorescently labelled anionic dextran.[74] A second generation of these nanotubes was created to stabilize the tubes and thereby expand the scope of this material as a delivery vehicle.[75] By introducing metal-binding ligands into this nanotube using heterotrimers composed of the coiled-coil peptides **p2L** (*vide supra*) and **TriNL**, the tube stability was increased in a metal-dependent manner. These tubes were still able to include dextrans within their interior, with inclusion of His-tagged fluorophores at either the ends of the tubes, or throughout, with the addition of metal ions.[70] Montclare and coworkers have created coiled-coil nanofibers ($\mathbf{C_{CC}^5}$) based on the cartilage oligomeric matrix protein that encapsulate BMS493, a small molecule used for osteoarthritis treatment.[76] BMS493 readily degrades and isomerizes, making delivery of this drug difficult. Trapping the drug in the coiled-coil nanofibers was found to stabilize this therapeutic.

Hydrogels have also been investigated for cargo binding and delivery. For instance, Montclare and coworkers designed a hydrogel from the coiled-coil peptide **Q** for controlled drug release.[77] This hydrogel was successful as a vehicle for sustained release of curcumin. Alternatively, Zhong and coworkers designed a pH-responsive nanogel by conjugating helices of a heterocoiled-coil to hyaluronic acid (**HA-K3** and **HA-E3**).[78] The hyaluronic acid targeted breast cancer cells with overexpressed CD44 receptors, and when saporin, a ribosome inactivating protein, was included as cargo, the nanogel was reported to exhibit potent anticancer activity.

These efforts demonstrate an impressive array of materials with the capacity to bind both small molecules and proteins. Of particular interest is the inclusion of proteins within 3D crystals and filaments. The enhanced thermal stability of the protein guests points to interesting applications in room temperature storage of biopharmaceuticals and enzymes. The ability to bind and release cargo within coiled-coil materials and interact with cells, as demonstrated by the **SAGEs** cages, brings the use of coiled-coil materials as drug delivery vehicles closer to reality.

Three-dimensional Cell Culturing. Creating biocompatible three-dimensional scaffolds has been a major goal in support of tissue engineering. The extracellular matrix is very structurally complex, and 2D cell culturing is severely limited in mimicking *in vivo* settings.[79–81] While natural 3D scaffolds like Matrigel are commonly used, batch to batch variation and an ill-defined composition limit the tunability.[82]

Creating highly crosslinked 3D structures from sequence defined coiled-coil peptides has been used to circumvent these issues. Woolfson and coworkers, for instance, have designed coiled-coil sequences that form hydrogels through sticky ends using hydrogen bonding or hydrophobic interactions (**hSAFs**).[83,84] This, in turn, allowed them to control the strength of the hydrogel through heating. Rat adrenal pheochromocytoma cells and neural stem cells were seeded onto the gels, and gel penetration and subsequent differentiation was observed. In an alternate strategy, Kobatake and coworkers developed a conjugate (**CUBE**) between a tetrameric, antiparallel coiled-coil and elastin-like polypeptide to prepare a hydrogel. By heating (37 °C) **CUBE**, the ELP segments aggregated leading to a crosslinked hydrogel.[85] Upon introducing the cell adhesion sequence RGD and heparin-binding angiogenic growth factors into these hydrogels, HUVEC cells that were encapsulated in the 3D network were found to undergo angiogenesis, a process that is usually only observed within 3D matrices (Figure 9A). Alternatively, the George lab used a triblock strategy whereby two GCN4 coiled-coil peptides were linked with a random coil peptide containing the RGDS sequence. Strategically placed cysteine residues allowed for hydrogel formation through disulfide bond formation.[86] Added human marrow stem cells adhered to the hydrogel and subsequent neovascularization was observed. Dexter and coworkers modified the **AFD19** sequence described above with an S16K substitution so that a hydrogel could form at physiological pH.[87] This gel exhibited low cell toxicity, and was suitable for the growth of mouse fibroblast cells with a spread morphology.

While hydrogels remain the most prevalent type of three-dimensional networks based on coiled-coil sequences, Chmielewski and Jorgensen have developed a coiled-coil-based assembly (**TriCross**) that achieved the same crosslinked morphology while not exhibiting gelation.[33] Their assembly design, as described above, was based on a trimeric GCN4 leucine zipper, and used metal-ligand interactions at both the center and termini of the peptide. The conditions for assembly enabled HeLa cells to be added during the process to fully encapsulate the cells into the 3D matrix (Figure 9B). The cells showed excellent viability within the scaffold after 6 days, and cells released from the matrix with a mild EDTA treatment demonstrated high viability. The reversibility of this matrix under mild conditions has promise for the isolation of grown tissue.

Overall, the examples of coiled-coil crosslinked assemblies provided above demonstrate significant potential as mimics of the extracellular matrix for tissue engineering. The coiled-coil 3D matrices have great potential for implantable materials and for 3D patterning of cell/tissue/material constructs. The ability to reverse the assembly process to release tissue in a chelation-controlled manner, as demonstrated by **TriCross**, could be particularly useful in regenerative medicine applications.

Vaccine development and Immunology. Vaccines derived from coiled-coil assemblies have recently been developed for multivalent display of epitopes. These potential vaccine candidates show great promise when compared to soluble antigens for their ability to present a high level of antigens and elicit a stronger immune response.[88] For instance, Burkhard developed a nanoparticle with dodecahedral symmetry that was composed of a trimeric coiled-coil sequence linked to a pentameric coiled-coil sequence via a disulfide (**SAPNs**, Figure 10).[89,90] The solvent exposed terminus of the peptides within the nanoparticle was functionalized with the coiled-coil of the HIV surface protein gp41 to create an adjuvant-free immunogen.[89,91] A follow up study functionalized the particles with a spike protein epitope for SARS-CoV-1. Animal studies with these nanoparticles revealed potent neutralization activity.[92]

Since then, Burkhard's nanoparticle design has been used for a number of vaccine candidates. Lanar and coworkers, for instance, have installed B and T cell epitopes for malaria within the nanoparticle.[93, 94] Mouse studies showed protection against the malaria parasite *P. berghei* for up to six months with just the B cell epitope, whereas the combined epitopes doubled the length of protection, and also provided protection against transgenic *P. berghei*. Bissati and coworkers have also used these nanoparticles for *toxoplasma gondii* infection,[95–97] whereas Khan and coworkers used this platform to generate vaccine candidates against avian influenza,[98,99] seasonal influenza,[100] and an infectious bronchitis virus.[101] Indeed, this simple coiled-coil platform allows for facile tunability and shows great promise for future vaccine development.

Other coiled-coil assemblies have also been used for multivalent display of epitopes for use in potential vaccines. The Robinson lab, for example, designed a virus-like nanoparticle

using a coiled-coil peptide with a lipid tail, rather than the two coiled-coils used by Burkhard.[102] The outer shell of the nanoparticle was decorated with an HIV-1 sequence to illicit an immune response. Collier and coworkers used a CD4+ T-cell epitope-containing coiled-coil that assembles into nanofibers and elicits an immune response in mice.[103] This material was subsequently optimized by controlling the length of the nanofibers.[104] Corradin and coworkers used the coiled-coil domains of malaria epitopes and connected them with non-immunogenic linkers.[105] A cellular assay revealed inhibition of parasite growth in the presence of this assembly. Finally, using Woolfson's **SAGEs** described above, Davidson and coworkers decorated the cages with tetanus toxoid, ovalbumin, or hemagglutinin antigens.[106] Both *in vitro* and *in vivo* studies revealed immune responses following exposure to these nanocages.

Coiled-coil nanoparticles are an excellent vehicle for the 3D display of multivalent ligands. This feature is ideal for applications in vaccine development. Additionally, striking animal data is emerging to support the future application of these strategies in humans.

3. Conclusions

The coiled-coil motif has been an area of great interest for *de novo* peptide design. More recently this building block has been successfully employed to generate a wide range of materials with morphologies that include fibrils, fibers, cages, crystals, tetrahera, nanotubes, hydrogels and 3D matrices. Because of the programmability of coiled-coils, assemblies can be formed through a number of methods, including complementary ionic and metal-ligand interactions, and through covalent chemistry. While significant progress has been made in the development of coiled-coil biomaterials, the rules for the various types of assembly are still being elucidated, an area where machine learning approaches may be useful in the future. Whereas we have focused in this review on biomedical applications, a growing number of coiled-coil assemblies are also being used as conductive materials, including photoelectronically active fibrils and conductive nanofilaments using metalloproteins within a coiled-coil assembly.[107–111]

With many of the systems described herein having proven use in protein storage, cargo delivery, cell culture and vaccine development, the future potential of coiled-coil materials to have significant biomedical impact is highly promising. Future applications of coiled-coil materials could include the combination of multi-layered nanoscale coiled-coil assemblies with cargo loading and cell interactions for the delivery of biological cargoes, such as therapeutic proteins and oligonucleotides. Importantly, such biopharmaceuticals could also be stabilized for room temperature storage and transport through inclusion within coiled-coil crystals and tubes. Additionally, the 3D patterning of cells and the peptide biomaterials, in a reversible manner when needed, would be a powerful means to create complex tissues for drug testing and as implantable materials for *in vivo* use.

Conflicts of interest

The authors declare no conflicts of interest.

Acknowledgements

This work was supported by the National Science Foundation through Grant CHE-2108722.

References

1 X. Liu, C. Wang and Z. Liu, *Adv. Healthc. Mater.*, 2018, 7.
2 A. W. Xie and W. L. Murphy, *Curr. Opin. Biomed. Eng.*, 2019, **10**, 1–10.
3 A. K. Gaharwar, I. Singh and A. Khademhosseini, *Nat. Rev. Mater.*, 2020, **5**, 686–705.
4 K. H. A. Lau, *Biomater. Sci.*, 2014, **2**, 627–633.
5 J. Durão and L. Gales, *Curr. Org. Chem.*, 2015, **19**, 1874–1881.
6 M. P. Hendricks, K. Sato, L. C. Palmer and S. I. Stupp, *Acc. Chem. Res.*, 2017, **50**, 2440–2448.
7 K. Lin, D. Zhang, M. H. Macedo, W. Cui, B. Sarmento and G. Shen, *Adv. Funct. Mater.*, 2019, **29**, 1804943.
8 M. K. Yadav, J. E. Redman, L. J. Leman, J. M. Alvarez-Gutiérrez, Y. Zhang, C. D. Stout and M. R. Ghadiri, *Biochemistry*, 2005, **44**, 9723–9732.
9 W. M. Dawson, F. J. O. Martin, G. G. Rhys, K. L. Shelley, R. L. Brady and D. N. Woolfson, *Chem. Sci.*, 2021, **12**, 6923–6928.
10 P. B. Harbury, T. Zhang, P. S. Kim and T. Alber, *Science (80-.).*, 1993, **262**, 1401–1407.
11 N. R. Zaccai, B. Chi, A. R. Thomson, A. L. Boyle, G. J. Bartlett, M. Bruning, N. Linden, R. B. Sessions, P. J. Booth, R. L. Brady and D. N. Woolfson, *Nat. Chem. Biol.*, 2011, **7**, 935–941.
12 J. Liu, Q. Zheng, Y. Deng, C. S. Cheng, N. R. Kallenbach and M. Lu, *Proc. Natl. Acad. Sci. U. S. A.*, 2006, **103**, 15457–15462.
13 J. M. Mason, M. A. Schmitz, K. M. Müller and K. M. Arndt, *Proc. Natl. Acad. Sci. U. S. A.*, 2006, **103**, 8989–8994.
14 M. ElGamacy and B. Hernandez Alvarez, *Curr. Opin. Struct. Biol.*, 2021, **68**, 224–234.
15 F. Lapenta, J. Aupič, Ž. Strmšek and R. Jerala, *Chem. Soc. Rev.*, 2018, **47**, 3530–3542.
16 D. M. Raymond and B. L. Nilsson, *Chem. Soc. Rev.*, 2018, **47**, 3659–3720.
17 W. M. Park, *Int. J. Mol. Sci.*, , DOI:10.3390/ijms21103584.
18 R. W. Curtis and J. Chmielewski, *Pept. Sci.*, 2021, **113**, e224190.
19 J. Utterström, S. Naeimipour, R. Selegård and D. Aili, *Adv. Drug Deliv. Rev.*, 2021, **170**, 26–43.
20 N. C. Burgess, T. H. Sharp, F. Thomas, C. W. Wood, A. R. Thomson, N. R. Zaccai, R. L. Brady, L. C. Serpell and D. N. Woolfson, *J. Am. Chem. Soc.*, 2015, **137**, 10554–10562.
21 C. Xu, R. Liu, A. K. Mehta, R. C. Guerrero-Ferreira, E. R. Wright, S. Dunin-Horkawicz, K. Morris, L. C. Serpell, X. Zuo, J. S. Wall and V. P. Conticello, *J. Am. Chem. Soc.*, 2013, **135**,

15565–15578.
22 J. Hume, J. Sun, R. Jacquet, P. D. Renfrew, J. A. Martin, R. Bonneau, M. L. Gilchrist and J. K. Montclare, *Biomacromolecules*, 2014, **15**, 3503–3510.
23 Y. Zimenkov, S. N. Dublin, R. Ni, R. S. Tu, V. Breedveld, R. P. Apkarian and V. P. Conticello, *J. Am. Chem. Soc.*, 2006, **128**, 6770–6771.
24 N. L. Fletcher, C. V. Lockett and A. F. Dexter, *Soft Matter*, 2011, **7**, 10210–10218.
25 M. Nambiar, L. S. Wang, V. Rotello and J. Chmielewski, *J. Am. Chem. Soc.*, 2018, **140**, 13028–13033.
26 M. Meleties, P. Katyal, B. Lin, D. Britton and J. K. Montclare, *Soft Matter*, 2021, **17**, 6470–6476.
27 Y. Tian, F. B. Polzer, H. V. Zhang, K. L. Kiick, G. Saven and D. J. Pochan, *Biomacromolecules*, 2018, **19**, 4286–4298.
28 Y. Tian, H. V. Zhang, K. L. Kiick, J. G. Saven and D. J. Pochan, *Chem. Mater.*, 2018, **30**, 8510–8520.
29 M. V Tsurkan and M. Y. Ogawa, *Chem. Commun.*, 2004, 2092–2093.
30 M. V. Tsurkan and M. Y. Ogawa, *Biomacromolecules*, 2007, **8**, 3908–3913.
31 I. M. M. Carvalho and M. Y. Ogawa, *J. Braz. Chem. Soc.*, 2010, **21**, 1390–1394.
32 M. Nepal, M. J. Sheedlo, C. Das and J. Chmielewski, *J. Am. Chem. Soc.*, 2016, **138**, 11051–11057.
33 M. D. Jorgensen and J. Chmielewski, *J. Pept. Sci.*, 2021, e3302.
34 R. W. Curtis, K. L. Scrudders, J. R. W. Ulcickas, G. J. Simpson, S. T. Low-nam and J. Chmielewski, *ACS Biomater. Sci. Eng.*, 2022, **8**, 1860–1866.
35 N. A. Tavenor, M. J. Murnin and W. S. Horne, *J. Am. Chem. Soc.*, 2017, **139**, 2212–2215.
36 K. A. Scheib, N. A. Tavenor, M. J. Lawless, S. Saxena and W. S. Horne, *Chem. Commun.*, 2019, **55**, 7752–7755.
37 V. A. Morozov and M. Y. Ogawa, *Inorg. Chem.*, 2013, **52**, 9166–9168.
38 D. V. Zaytsev, V. A. Morozov, J. Fan, X. Zhu, M. Mukherjee, S. Ni, M. A. Kennedy and M. Y. Ogawa, *J. Inorg. Biochem.*, 2013, **119**, 1–9.
39 S. N. Dublin and V. P. Conticello, *J. Am. Chem. Soc.*, 2008, **130**, 49–51.
40 P. Anzini, C. Xu, S. Hughes, E. Magnotti, T. Jiang, L. Hemmingsen, B. Demeler and V. P. Conticello, *J. Am. Chem. Soc.*, 2013, **135**, 10278–10281.
41 F. Thomas, N. C. Burgess, A. R. Thomson and D. N. Woolfson, *Angew. Chemie - Int. Ed.*, 2016, **55**, 987–991.
42 D. Wu, N. Sinha, J. Lee, B. P. Sutherland, N. I. Halaszynski, Y. Tian, J. Caplan, H. V. Zhang, J. G. Saven, C. J. Kloxin and D. J. Pochan, *Nature*, 2019, **574**, 658–662.
43 K. Kim, C. J. Kloxin, G. Saven and D. J. Pochan, *ACS Appl. Mater. Interfaces*, 2021, **13**, 26339–26351.
44 L. Jiang, X. Zuo, J. Li, N. J. Traaseth and K. Kirshenbaum, *Angew. Chemie Int. Ed.*, 2022, e202201895.
45 H. Gradišar, S. Božič, T. Doles, D. Vengust, I. Hafner-Bratkovič, A. Mertelj, B. Webb, A. Šali, S. Klavžar and R. Jerala, *Nat. Chem. Biol.*, 2013, **9**, 362–366.
46 J. Aupič, Ž. Strmšek, F. Lapenta, D. Pahovnik, T. Pisanski, I. Drobnak, A. Ljubetič and R. Jerala, *Nat. Commun.*, 2021, **12**, 1–12.
47 L. J. Dooling, M. E. Buck, W. Bin Zhang and D. A. Tirrell, *Adv. Mater.*, 2016, **28**, 4651–4657.
48 L. J. Dooling and D. A. Tirrell, *ACS Cent. Sci.*, 2016, **2**, 812–819.
49 W. Shen, K. Zhang, J. A. Kornfield and D. A. Tirrell, *Nat. Mater.*, 2006, **5**, 153–158.
50 N. E. Domeradzka, M. W. T. Werten, F. A. De Wolf and R. De Vries, *Biomacromolecules*, 2016, **17**, 3893–3901.
51 M. Zhou, D. Bentley and I. Ghosh, *J. Am. Chem. Soc.*, 2004, **126**, 734–735.
52 S. Dånmark, C. Aronsson and D. Aili, *Biomacromolecules*, 2016, **17**, 2260–2267.
53 I. Tunn, A. S. De Léon, K. G. Blank and M. J. Harrington, *Nanoscale*, 2018, **10**, 22725–22729.
54 I. Tunn, M. J. Harrington and K. G. Blank, *Biomimetics*, 2019, **4**, 1–17.
55 K. M. Polizzi, A. S. Bommarius, J. M. Broering and J. F. Chaparro-Riggers, *Curr. Opin. Chem. Biol.*, 2007, **11**, 220–225.
56 A. Butreddy, K. Y. Janga, S. Ajjarapu, S. Sarabu and N. Dudhipala, *Int. J. Biol. Macromol.*, 2021, **167**, 309–325.
57 R. Juliano, *Biochem. Soc.*, 2007, **35**, 29–31.
58 B. J. Boyd, C. A. S. Bergström, Z. Vinarov, M. Kuentz, J. Brouwers, P. Augustijns, M. Brandl, A. Bernkop-Schnürch, N. Shrestha, V. Préat, A. Müllertz, A. Bauer-Brandl and V. Jannin, *Eur. J. Pharm. Sci.*, 2019, **137**, 104967.
59 M. Z. Ahmad, M. Rizwanullah, J. Ahmad, M. Y. Alasmary, M. H. Akhter, B. A. Abdel-Wahab, M. H. Warsi and A. Haque, *Int. J. Polym. Mater. Polym. Biomater.*, 2022, **71**, 602–623.
60 D. J. Glover, S. Lim, D. Xu, N. B. Sloan, Y. Zhang and D. S. Clark, *ACS Synth. Biol.*, 2018, **7**, 2447–2456.
61 H. Dong, N. Dube, J. Y. Shu, J. W. Seo, L. M. Mahakian, K. W. Ferrara and T. Xu, *ACS Nano*, 2012, **6**, 5320–5329.
62 J. Y. Shu, R. Lund and T. Xu, *Biomacromolecules*, 2012, **13**, 1945–1955.
63 N. Dube, J. Y. Shu, H. Dong, J. W. Seo, E. Ingham, A. Kheirolomoom, P. Y. Chen, J. Forsayeth, K. Bankiewicz, K. W. Ferrara and T. Xu, *Biomacromolecules*, 2013, **14**, 3697–3705.
64 N. Dube, J. W. Seo, H. Dong, J. Y. Shu, R. Lund, L. M. Mahakian, K. W. Ferrara and T. Xu, *Biomacromolecules*, 2014, **15**, 2963–2970.
65 J. W. Seo, J. C. Ang, L. M. Mahakian, S. Tam, B. Fite, E. S. Ingham, J. Beyer, J. Forsayeth, K. S. Bankiewicz, T. Xu and K. W. Ferrara, *J. Control. Release*, 2015, **220**, 51–60.
66 J. Ang, D. Ma, R. Lund, S. Keten and T. Xu, *Biomacromolecules*, 2016, **17**, 3262–3267.
67 J. Ang, D. Ma, B. T. Jung, S. Keten and T. Xu, *Biomacromolecules*, 2017, **18**, 3572–3580.
68 Y. Xue, B. T. Jung and T. Xu, *Pept. Sci.*, 2020, **112**, e24117.
69 Y. Assal, Y. Mizuguchi, M. Mie and E. Kobatake, *Bioconjug. Chem.*, 2015, **26**, 1672–1677.
70 J. M. Fletcher, R. L. Harniman, F. R. H. Barnes, A. L. Boyle, A. Collins, J. Mantell, T. H. Sharp, M. Antognozzi, P. J.

Booth, N. Linden, M. J. Miles, R. B. Sessions, P. Verkade and D. N. Woolfson, *Science (80-.).*, 2013, **340**, 595–599.
71 J. F. Ross, A. Bridges, J. M. Fletcher, D. Shoemark, D. Alibhai, H. E. V. Bray, J. L. Beesley, W. M. Dawson, L. R. Hodgson, J. Mantell, P. Verkade, C. M. Edge, R. B. Sessions, D. Tew and D. N. Woolfson, *ACS Nano*, 2017, **11**, 7901–7914.
72 J. L. Beesley, H. E. Baum, L. R. Hodgson, P. Verkade, G. S. Banting and D. N. Woolfson, *Nano Lett.*, 2018, **18**, 5933–5937.
73 A. J. Gormley, R. Chandrawati, A. J. Christofferson, C. Loynachan, C. Jumeaux, A. Artzy-Schnirman, D. Aili, I. Yarovsky and M. M. Stevens, *Chem. Mater.*, 2015, **27**, 5820–5824.
74 M. Nambiar, M. Nepal and J. Chmielewski, *ACS Biomater. Sci. Eng.*, 2019, **5**, 5082–5087.
75 M. D. Jorgensen and J. Chmielewski, *ACS Omega*, 2022, **7**, 20945–20951.
76 L. Yin, A. S. Agustinus, C. Yuvienco, T. Minashima, N. L. Schnabel, T. Kirsch and J. K. Montclare, *Biomacromolecules*, 2018, **19**, 1614–1624.
77 L. K. Hill, M. Meleties, P. Katyal, X. Xie, E. Delgado-Fukushima, T. Jihad, C. F. Liu, S. O'Neill, R. S. Tu, P. D. Renfrew, R. Bonneau, Y. Z. Wadghiri and J. K. Montclare, *Biomacromolecules*, 2019, **20**, 3340–3351.
78 L. Ding, Y. Jiang, J. Zhang, H. A. Klok and Z. Zhong, *Biomacromolecules*, 2018, **19**, 555–562.
79 C. Frantz, K. M. Stewart and V. M. Weaver, *J. Cell Sci.*, 2010, **123**, 4195–4200.
80 S. A. Langhans, *Front. Pharmacol.*, 2018, **9**, 1–14.
81 T. Nii, K. Makino and Y. Tabata, *Cancers (Basel).*, 2020, **12**, 2754.
82 E. A. Aisenbrey and W. L. Murphy, *Nat. Rev. Mater.*, 2020, **5**, 539–551.
83 E. F. Banwell, E. S. Abelardo, D. J. Adams, M. A. Birchall, A. Corrigan, A. M. Donald, M. Kirkland, L. C. Serpell, M. F. Butler and D. N. Woolfson, *Nat. Mater.*, 2009, **8**, 596–600.
84 N. Mehrban, B. Zhu, F. Tamagnini, F. I. Young, A. Wasmuth, K. L. Hudson, A. R. Thomson, M. A. Birchall, A. D. Randall, B. Song and D. N. Woolfson, *ACS Biomater. Sci. Eng.*, 2015, **1**, 431–439.
85 Y. Mizuguchi, Y. Mashimo, M. Mie and E. Kobatake, *Biomacromolecules*, 2020, **21**, 1126–1135.
86 C. C. Huang, S. Ravindran, Z. Yin and A. George, *Biomaterials*, 2014, **35**, 5316–5326.
87 A. F. Dexter, N. L. Fletcher, R. G. Creasey, F. Filardo, M. W. Boehm and K. S. Jack, *RSC Adv.*, 2017, **7**, 27260–27271.
88 C. M. Snapper, *Front. Immunol.*, 2018, **9**, 598.
89 S. Raman, G. Machaidze, A. Lustig, U. Aebi and P. Burkhard, *Nanomedicine Nanotechnology, Biol. Med.*, 2006, **2**, 95–102.
90 T. A. P. F. Doll, R. Dey and P. Burkhard, *J. Nanobiotechnology*, 2015, **13**, 1–12.
91 N. Wahome, T. Pfeiffer, I. Ambiel, Y. Yang, O. T. Keppler, V. Bosch and P. Burkhard, *Chem. Biol. Drug Des.*, 2012, **80**, 349–357.
92 T. A. P. F. Pimentel, Z. Yan, S. A. Jeffers, K. V. Holmes, R. S. Hodges and P. Burkhard, *Chem. Biol. Drug Des.*, 2009, **73**, 53–61.
93 S. A. Kaba, C. Brando, Q. Guo, C. Mittelholzer, S. Raman, D. Tropel, U. Aebi, P. Burkhard and D. E. Lanar, *J. Immunol.*, 2009, **183**, 7268–7277.
94 S. A. Kaba, M. E. McCoy, T. A. P. F. Doll, C. Brando, Q. Guo, D. Dasgupta, Y. Yang, C. Mittelholzer, R. Spaccapelo, A. Crisanti, P. Burkhard and D. E. Lanar, *PLoS One*, 2012, **7**, e48304.
95 K. El Bissati, Y. Zhou, D. Dasgupta, D. Cobb, J. P. Dubey, P. Burkhard, D. E. Lanar and R. McLeod, *Vaccine*, 2014, **32**, 3243–3248.
96 K. El Bissati, Y. Zhou, S. M. Paulillo, S. K. Raman, C. P. Karch, C. W. Roberts, D. E. Lanar, S. Reed, C. Fox, D. Carter, J. Alexander, A. Sette, J. Sidney, H. Lorenzi, I. J. Begeman, P. Burkhard and R. McLeod, *npj Vaccines*, 2017, **2**, 1–11.
97 K. El Bissati, Y. Zhou, S. M. Paulillo, S. K. Raman, C. P. Karch, S. Reed, A. Estes, A. Estes, J. Lykins, P. Burkhard and R. McLeod, *Sci. Rep.*, 2020, **10**, 1–13.
98 S. Babapoor, T. Neef, C. Mittelholzer, T. Girshick, A. Garmendia, H. Shang, M. I. Khan and P. Burkhard, *Influenza Res. Treat.*, 2011, **2011**, 1–12.
99 J. Li, Z. Helal, B. Ladman, C. Karch, J. Gelb Jr, P. Burkhard and M. I. Khan, *J. Virol. Antivir. Res.*, 2018, **7**, 1–5.
100 C. P. Karch, J. Li, C. Kulangara, S. M. Paulillo, S. K. Raman, S. Emadi, A. Tan, Z. H. Helal, Q. Fan, M. I. Khan and P. Burkhard, *Nanomedicine Nanotechnology, Biol. Med.*, 2017, **13**, 241–251.
101 J. Li, Z. H. Helal, C. P. Karch, N. Mishra, T. Girshick, A. Garmendia, P. Burkhard and M. I. Khan, *PLoS One*, 2018, **13**, 1–17.
102 F. Boato, R. M. Thomas, A. Ghasparian, A. Freund-Renard, K. Moehle and J. A. Robinson, *Angew. Chemie - Int. Ed.*, 2007, 46, 9015–9018.
103 Y. Wu, P. K. Norberg, E. A. Reap, K. L. Congdon, C. N. Fries, S. H. Kelly, J. H. Sampson, V. P. Conticello and J. H. Collier, *ACS Biomater. Sci. Eng.*, 2017, **3**, 3128–3132.
104 C. N. Fries, Y. Wu, S. H. Kelly, M. Wolf, N. L. Votaw, S. Zauscher and J. H. Collier, *Adv. Mater.*, 2020, 32, 2003310.
105 S. Olugbile, V. Villard, S. Bertholet, A. Jafarshad, C. Kulangara, C. Roussilhon, G. Frank, G. W. Agak, I. Felger, I. Nebie, K. Konate, A. V. Kajava, P. Schuck, P. Druilhe, F. Spertini and G. Corradin, *Vaccine*, 2011, **29**, 7090–7099.
106 C. Morris, S. J. Glennie, H. S. Lam, H. E. Baum, D. Kandage, N. A. Williams, D. J. Morgan, D. N. Woolfson and A. D. Davidson, *Adv. Funct. Mater.*, 2019, **29**, 1807357.
107 D. E. Wagner, C. L. Phillips, W. M. Ali, G. E. Nybakken, E. D. Crawford, A. D. Schwab, W. F. Smith and R. Fairman, *Proc. Natl. Acad. Sci. U. S. A.*, 2005, **102**, 12656–12661.
108 B. Kokona, A. M. Kim, R. C. Roden, J. P. Daniels, B. J. Pepe-mooney, B. C. Kovaric, J. C. De Paula, K. A. Johnson and R. Fairman, *Biomacromolecules*, 2009, **10**, 1454–1459.
109 B. J. Pepe-Mooney, B. Kokona and R. Fairman, *Biomacromolecules*, 2011, **12**, 4196–4203.
110 J. C. Taggart, E. Z. Welch, M. F. Mulqueen, V. B. Dioguardi, A. G. Cauer, B. Kokona and R. Fairman, *Biomacromolecules*, 2014, **15**, 4544–4550.

111 Y. X. Chen, N. L. Ing, F. Wang, D. Xu, N. B. Sloan, N. T. Lam, D. L. Winter, E. H. Egelman, A. I. Hochbaum, D. S. Clark and D. J. Glover, *ACS Nano*, 2020, **14**, 6559–6569.

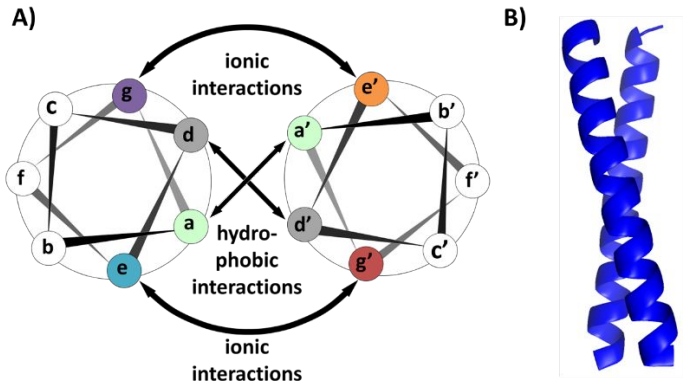

Figure 1. A) Helical wheel diagram of a coiled-coil dimer. B) 3D model of a dimeric coiled-coil

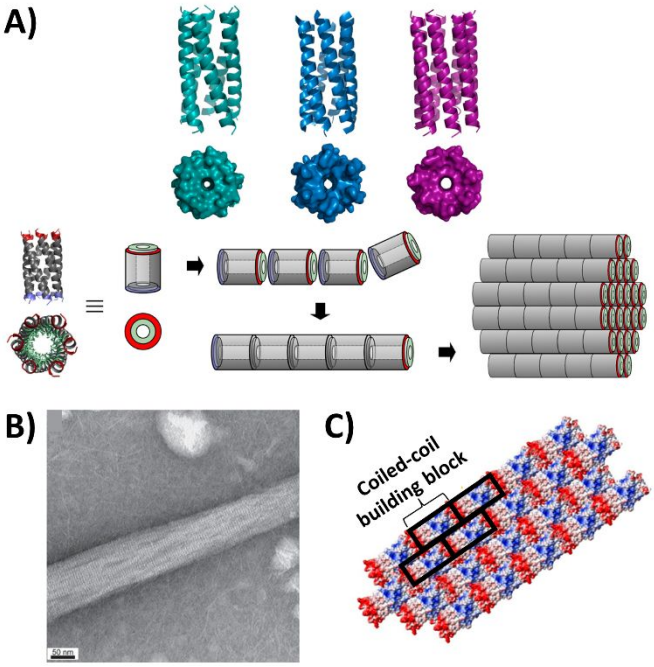

Figure 2. A) X-ray crystal structures of pentameric to heptameric coiled-coils and the proposed mechanism of fiber assembly. B) TEM micrograph of **7HSAP1** assembled in MES buffer (10 mM, pH 6.0). C) Schematic representation of peptide **Q** organization upon fiber formation in phosphate buffer (50 mM, pH 4). Reprinted with permission from ref. 15, 16, 17. Copyright 2013, 2014, 2015, American Chemical Society.

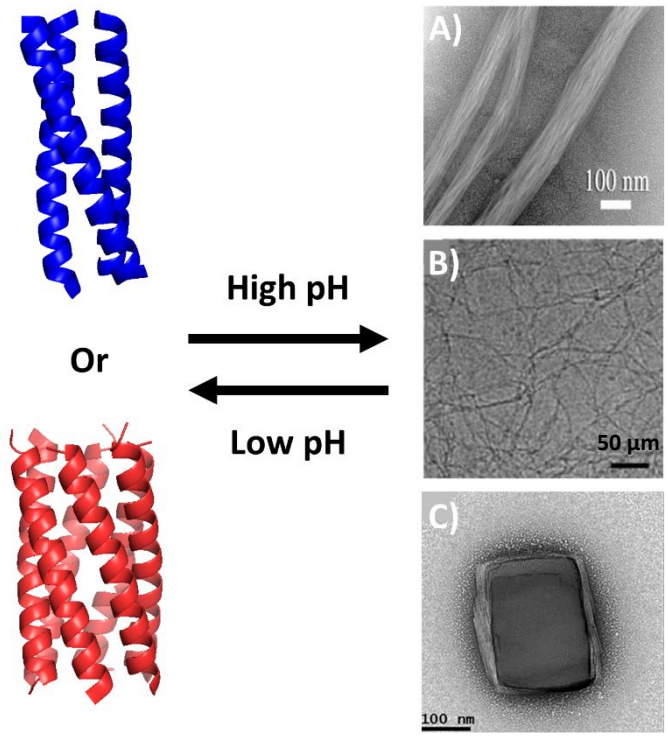

Figure 3. Transmission electron microscopy (TEM) images of reversible assemblies via pH. A) **TZ1H** fibers, B) **AFD19** fibers, and C) **TriByp3** assembly. Reprinted with permission from ref. 18, 19, 20. Copyright 2006, 2011, 2018, American Chemical Society and Royal Society of Chemistry.

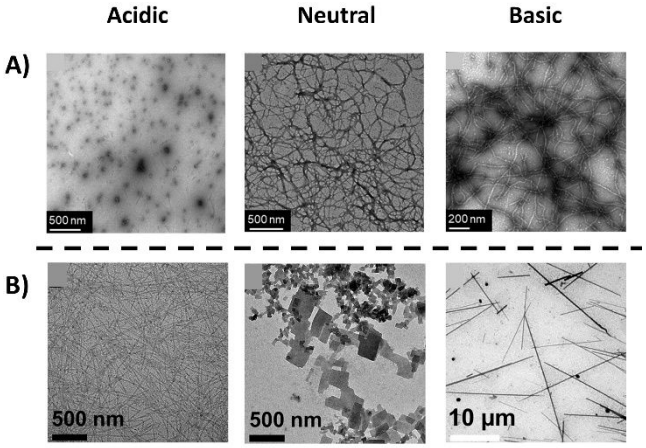

Figure 4. pH controlled assemblies. A) TEM of Montclare's assembled **Q** peptide in acidic, neutral, and basic conditions to produce either nanoparticles or fibers. B) TEM of Pochan's assembled peptide in acidic, neutral, and basic conditions to produce nanotubes, platelets, and needles, respectively. Reprinted with permission from ref. 21 and 22. Copyright 2018, 2021, American Chemical Society and Royal Society of Chemistry.

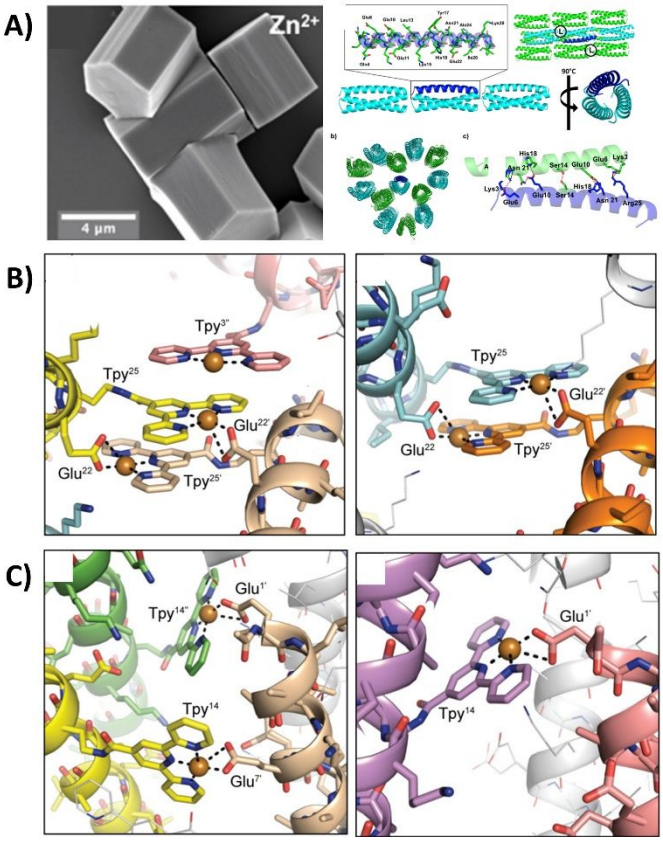

Figure 5. A) Scanning electron micrograph (SEM) of crystals of **p2L** (1 mM) with zinc ions (1 mM) and its corresponding crystal structure. B) Views of crystal structure of peptide **2** and C) peptide **3**. Reprinted with permission from ref. 27 and 30. Copyright 2016, 2017, American Chemical Society and Royal Society of Chemistry.

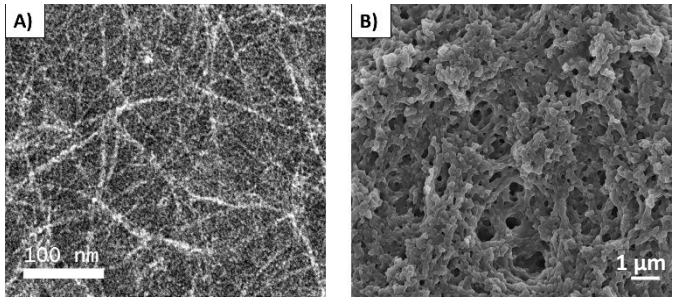

Figure 6. A) TEM image of **TZ1C2** fibrils (500 μM) in TAPS buffer (10 mM, pH 8.5) and NaCl (100 mM) before Cd(II) addition. B) SEM image of **TriCross** assembly with $ZnCl_2$ (1 mM each) in Dulbecco's Modified Eagle Medium (DMEM) with 10% fetal bovine serum (FBS) after 1 hr. Reprinted with permission from ref. 28 and 35. Copyright 2013, 2021, American Chemical Society and John Wiley and Sons.

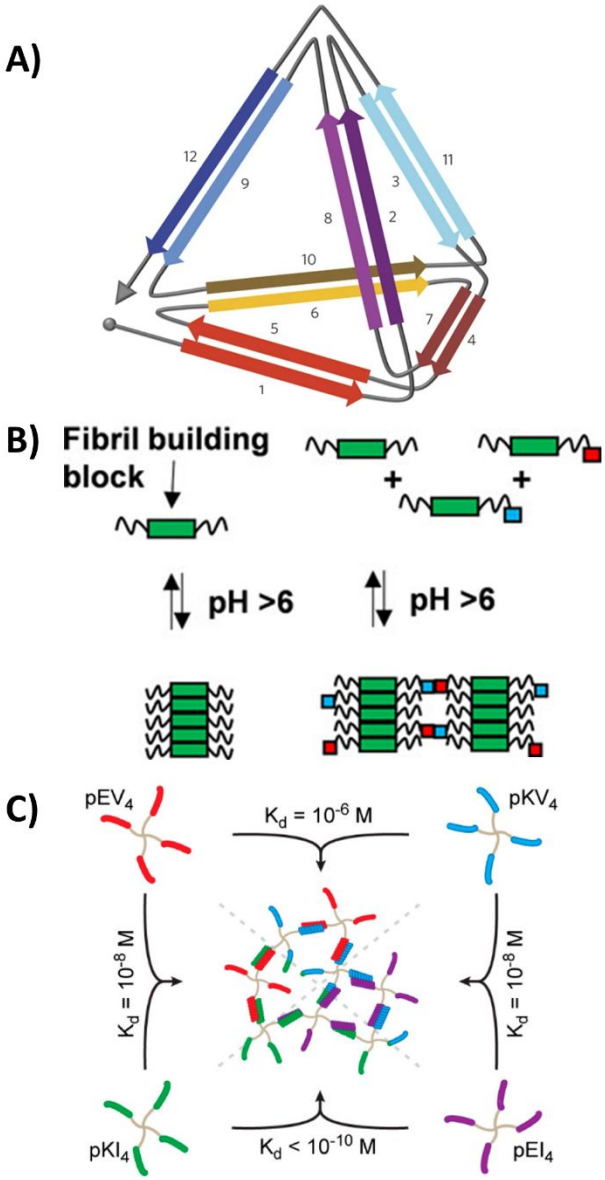

Figure 7. A) Schematic representation of the polypeptide path forming a tetrahedron. B) Cartoon diagram of fibril forming triblock with and without heterocoiled-coil installation. C) Relationship between coiled-coils and their corresponding binding affinities. Reprinted with permission from ref. 40, 45, 47. Copyright 2013, 2016, American Chemical Society and Springer Nature.

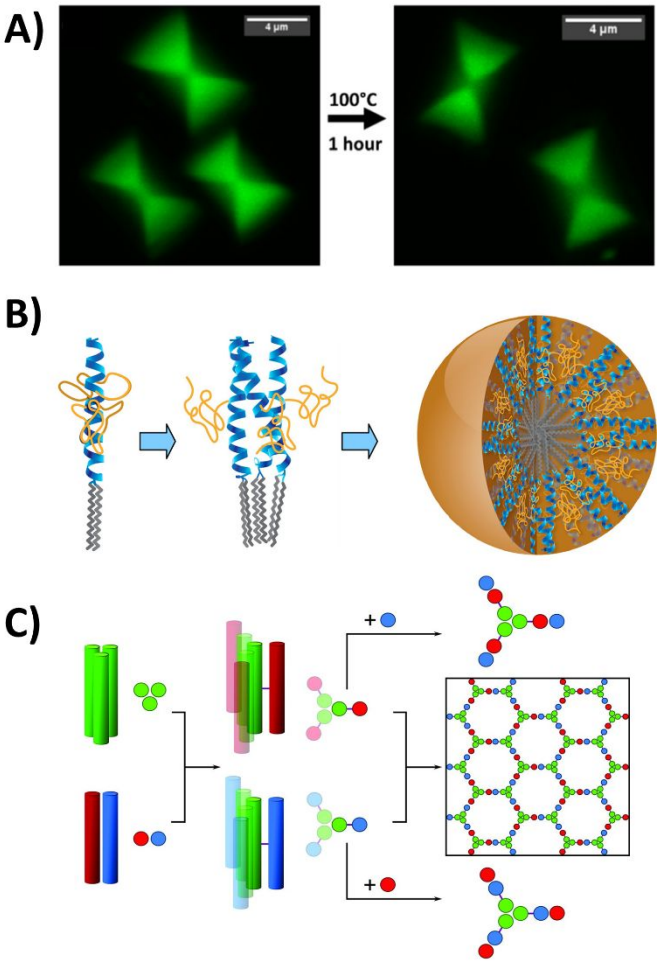

Figure 8. A) Stability of EGFP within **p2L** crystals. Fluorescence confocal images of Chmielewski's **p2L** crystals with enhanced green fluorescent protein guests before and after incubation at 100 °C for 1 hr. B) Schematic drawing of Xu's micelle, where the shell is composed of the 3-helix bundles and the core is composed of aliphatic chains. C) Design of Woolfson's peptide cages through disulfide linkages and heterocoiled-coils. Reprinted with permission from ref. 29, 56, 65. Copyright 2012, 2013, 2016, American Chemical Society and American Association for the Advancement of Science.

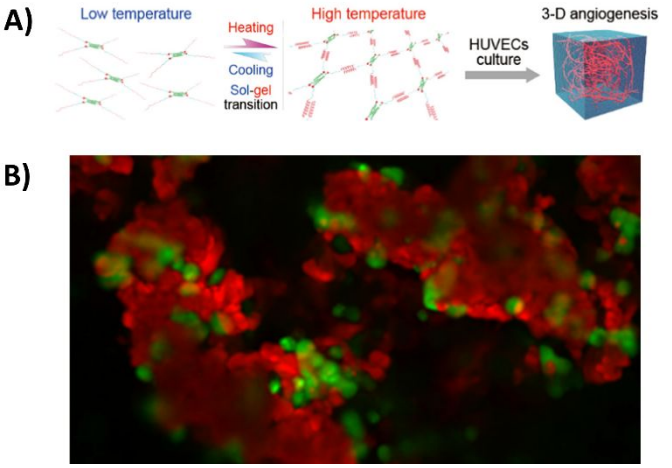

Figure 9. A) Schematic illustration of temperature-responsive hydrogel and the formation of blood vessels. B) Confocal microscopy image of live HeLa cells (green) encapsulated within the **TriCross** assembled labeled with Rh-His_6 (red) in DMEM with 10% FBS. Reprinted with permission from ref. 28, 80. Copyright 2020, 2021, American Chemical Society and John Wiley and Sons.

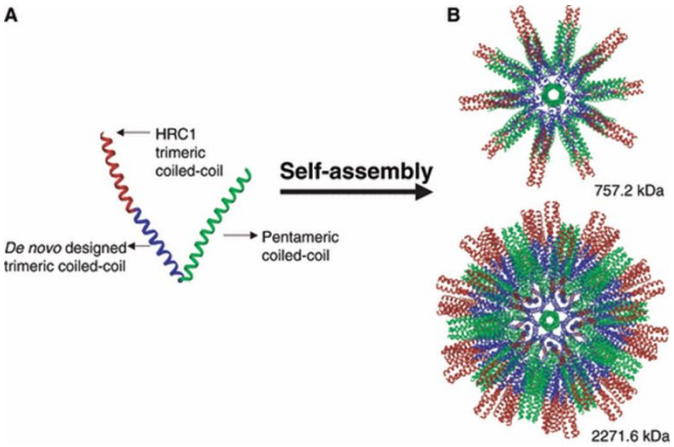

Figure 10. (A) 3D monomeric building block of **P6HRC1** composed of a modified pentameric coiled-coil domain from COMP (green) and trimeric de novo designed coiled-coil domain (blue) which is extended by the coiled-coil sequence of SARS HRC1 (red). (B) Computer models of the complete peptide nanoparticle **P6HRC1** with varying degrees of icosahedral symmetry. The calculated diameters of these particles are about 23 and 28 nm and the molecular weight 757 and 2271 kDa, respectively. Reprinted with permission from ref. 87. Copyright 2009, John Wiley and Sons.

ARTICLE

Table 1. Peptide sequences of this review with structures of unnatural modifications.

Peptide Name	Oligomeric State	Peptide Sequence
CC-Tet2-F	Tetramer	H_2N-NILQE(VKNILKE)(VKNILWE)(VKNILQE)VK-OH
CC-Hex-T	Hexamer	H_2N-(LKAIAQE)(LKAIAKE)(LKAIAWE)(LKAIAQE)-OH
7HSAP1	Heptamer	H_2N-(KLAQAVE)(KLARAVE)(KLAYANE)(KLARAVE)(KLAQAVE)-OH
Q subunit	Pentamer	-VKE(ITFLKNT)(APQMLRE)(LQETNAA)(LQDVREL)(LRQQSKL)-OH
TZ1H	Trimer	Ac-E(IAQ**H**EKE)(IQAIEKK)(IAQ**H**EYK)(IQAIEEK)(IAQ**H**KEK)IQAIK-OH
AFD19	Hexamer	Ac-(LKELAKV)(LHELAKL)(VSEALHA)-OH
TriByp1	Trimer	Ac-(MKQIEDK)(IEEIL**B**K)(IYHIENE)(IARIKKL)IGE-NH_2
TriByp2	Trimer	Ac-(MKQIEDK)(IEEIL**B**K)(IYHIE**B**E)(IARIKKL)IGE-NH_2
TriByp3	Trimer	Ac-(MKQIE**B**K)(IEEIL**B**K)(IYHIE**B**E)(IARIKKL)IGE-NH_2
AQ-Pal14	Dimer	Ac-K(IEALEGK)(IEALE**Pal**K)(IEACEGK)(IEALEGK)G-NH_2
H21	Dimer	Ac-K(IEALEGK)$_2$(IEALE**H**K)(IEALEGK)G-NH_2
p2L (x = S) **TriCross** (x = B)	Trimer	**NTA**-G(MKQIEDK)(IEEILxK)(IYKIENE)(IARIKKL)IGEG**HH**-NH_2
1 (Horne)	Dimer	Ac-E(IAALK**Tpy**E)(NAALKEE)(IAALKKE)(IAAL**Tpy**KG)-NH_2
2 (Horne)	Trimer	Ac-E(I**Tpy**AIKKE)(IEAIKKE)(IAEIKKE)(IA**Tpy**IKK)-NH_2
3 (Horne)	Tetramer	Ac-E(LAAIKEE)(LAAIK**Typ**E)(LAAIKQE)(LAAIKQ)-NH_2
TZ1C2	Trimer	Ac-E(IAQIEEE)(**C**QAIEER)(IAQIEYR)(IQAIEEK)(**C**AQIKEK)IQAIK-NH_2
CC-Hex-T + co	Hexamer	H_2N-(**C**KAIAKE)(LKAIAYE)(LKAIAKE)(LKAIAKQ)-**SBzl**
Peptide 1 (Pochan)	Tetramer	**Mal**-(DEKIKNM)(ADQIKHM)(AWMIDRM)(AEKIDRE)A-NH_2
Peptide 2 (Pochan)	Tetramer	H_2N-**C**(DEEIRRM)(AEEIRQM)(AERIQQM)(AEQIQQE)A-NH_2
4A	Dimer	Ac-WE(NAKLENI)(VARLEND)(NANLEKD)(IANLEKD)(IANLERD)VAR-**Az**
4B	Dimer	**az**-NT(VKELKNY)(IQELEER)(NAELKNL)(KEHLKFA)(KAELEFE)LAA-NH_2
EPE subunit	Pentamer	-APQM(LRELQET)(NAALQDV)(RELLRQQ)(VKEITFL)(KVTVMES)DAS-
PC10P subunit	Pentamer	-(APQMLRE)(LQETNAA)(LQDVREL)(LRQQVKE)(ITFLKNT)(VMESDAS)-
AC10A subunit	Tetramer	-(SGDLENE)(VAQLERE)(VRSLEDE)(AAELEQK)(VSRLKNE)(IEDLKAE)-
C_2-S^H_{48}-C_2-D^A subunit	Dimer	-LEIR(AAFLRQR)(NTALRTE)(VAELEQE)(VQRLENE)(VSQYETR)(YGPLGGG)KG-OH
C_2-S^H_{48}-C_2D^B subunit	Dimer	-LEIE(AAFLERE)(NTALETR)(VAELRQR)(VQRLRNR)(VSQYRTR)(YGPLGGG)KG-OH
EZ (x = E) **KZ** (x = K)	Dimer	H_2N-(AQALxKx)(LQALxKx)(LQALxWx)(LQALxKx)LSGSGC-OH
EV	Dimer	H_2N-(EVSALEK)(EVSALEK)(ENSALEW)(EVSALEK)**C**-OH
EI	Dimer	H_2N-**C**(KVSALKE)(KVSALKE)(KNSALKW)(KVSALKE)-OH
KV	Dimer	H_2N-(EIAALEK)(EIAALEK)(ENAALEW)(EIAALEK)**C**-OH
KI	Dimer	H_2N-**C**(KIAALKE)(KIAALKE)(KNAALKW)(KIAALKE)-OH
A_{4H3}	Dimer	Ac-CGG(EIAALE**H**)(EIAALE**H**)(ENAALE**H**)(EIAALEQ)GG-NH_2
B_{4H3}	Dimer	Ac-GG(KIAALK**H**)(KIAALK**H**)(KNAALK**H**)(KIAALKQ)GGC-NH_2
EE subunit	Dimer	-(IAALEKE)$_3$-
KK subunit	Dimer	-(LAAIKEK)$_3$-
1coi-dC18-PEG2K subunit	Trimer	-E(VEALEKK)(VAALESK)(VQALEKK)(VEALEHG)-
CC-Tri3	Trimer	Ac-G(EIAAIKK)(EIAAIKQ)(EIAAIKQ)GYG-NH_2
CC-DiA (x = E, y = W) **CC-DiB** (x = K, y = Y)	Dimer	Ac-G(XIAALXK)(XNAALXQ)(XIAALXQ)GyW-NH_2
JR2EC (x = E) **JR2KC** (x = K)	Dimer	H_2N-N(AADLxKA)(IxALxKH)(LxAKGP**C**)(DAAQLxK)(QLxQAFx)AFxRAG-NH_2
TriNL	Trimer	Ac-(MKQIEDK)(IEEILSK)(IYKIENE)(IARIKKL)IGE-NH_2
E3	Dimer	H_2N-GY(EIAALEK)$_3$GC-OH
K3	Dimer	H_2N-GY(KIAALKE)$_3$GC-OH
hSAF x = A/Q, y = A/Q, z = I/N	Dimer	H_2N-K(IxxLKyK)(ZxxLKyE)(IxxLExE)(yxxLEx)-OH
bRGD-CUBE	Tetramer	H_2N-$(AVGP)_{42}$-D_{88}-CGGNGEPRGDTYRAY-GN[(ADELYRM)(LDALREH)(LQSLRRK)]$_2$LRSG-OH
SAPN template	Trimer and Pentamer	Ac-DEM(LRELQET)(NAALQDV)(RELLRQQ)(VKQITFL)KCLLM-GG-RLLCR(LEELERR)(LEELERR)(LEELERR)-NH_2
CpA	Dimer	Ac-(CKQLEDK)(IEELLSK)-AA-(CKQLEDK)(IEELLSK)-NH_2
γPFD	Dimer	H_2N- MVNEVIDINEAVRAYIAQIEGLRAEIGRLDATIATLRQSLATLKSLKTLGEGKTVLVPVGSIAQVEMKVEKMDKVVVSVGQ NISAELEYEEALKYIEDEIKKLLTFRLVLEQAIAELYAKIEDIAEAQQTSEEEKAEEENEEKAE-OH